Physica B 406 (2011) 2200–2205

Contents lists available at ScienceDirect

Physica B

journal homepage: www.elsevier.com/locate/physb

Tuning the growth of ZnO nanowires

Z. Guo [a,b,c], C. Andreazza-Vignolle [a,*], P. Andreazza [a], T. Sauvage [d], D.X. Zhao [b], Y.C. Liu [e], B. Yao [b], D.Z. Shen [b], X.W. Fan [b]

[a] Centre de Recherche sur la Matière Divisée, CRMD, UMR 6619, Université d'Orléans, CNRS, 1b rue de la férollerie, 45071 Orléans Cedex 2, France
[b] Key Laboratory of Excited State Processes, Changchun Institute of Optics, Fine Mechanics and Physics, Chinese Academy of Sciences, 3888 East Nan-Hu Road, Open Economic Zone, Changchun 130033, People's Republic of China
[c] Graduate School of the Chinese Academy of Sciences, Beijing 100049, People's Republic of China
[d] CEMHTI, UPR 3079 CNRS, 3a rue de la férollerie, 45071 Orléans Cedex 2, France
[e] Center for Advanced Optoelectronic Functional Material Research, Northeast Normal University, Changchun 130024, People's Republic of China

ARTICLE INFO

Article history:
Received 13 January 2011
Received in revised form
11 March 2011
Accepted 14 March 2011
Available online 23 March 2011

Keywords:
Tuning the size
ZnO nanowires
Hydrothermal method

ABSTRACT

ZnO nanowires (NWs) with different diameters were obtained by controlling the particles of ZnO sub-layer (SL) exploring hydrothermal method; the diameter of the epitaxial NWs could be tuned from 60 to 146 nm when using SL with a thickness of 70 nm. The thickness of the SL would influence the orientation of the NWs. The top agglomerate NWs could be formed on the SL with a thickness of 10 nm, and the NWs with better orientation were obtained using SL with a thickness of 70 nm. Well aligned ZnO NWs grew perpendicular to the completely stress released SL. The diameter of the NWs was also greatly influenced by the solution concentration; thus ultra fine (diameter ~11 nm) ZnO NWs were obtained through adjusting the solution concentration to 0.001 mol/L. Through our research, we also found that the growth rate of the NWs could also be influenced by the different polarity surface of the SL. In other words, the size of the ZnO NWs could be tuned exactly under optimal conditions.

1. Introduction

ZnO is a promising material for short-wavelength photonic device applications due to its direct wide band gap with a large exciton bounding energy of 60 MeV [1]. These properties make it a potentially useful photonic material for ultraviolet (UV) photodetectors [2,3] and other optoelectronic applications [4,5]. Furthermore, ZnO NWs are regarded as one of the most promising materials for nanoscale UV photodetector, UV laser diode and optical switch applications [5–8]. Especially, ZnO NWs or nanoneedles have attracted much attention as a field emitter due to their high aspect ratio, high mechanical stability and negative electron affinity [9–11]. The potential advantages of one dimensional ZnO NWs make the fabrication of ZnO based photoelectric devices an attractive prospect, as it would enable the fabrication of many small units without using much space. Nowadays, many methods have been used to synthesize ZnO nanostructures, including chemical vapor deposition [11], metal-organic chemical vapor deposition [12], solution-grown method [13], sol–gel synthesis method [14], electrochemistry deposition [15], physical vapor deposition [16] and laser-assisted growth method [17]. In order to fabricate nano-devices, the size and orientation of the NWs should be controlled exactly. Here, we report the factors influencing the size of the epitaxial ZnO NWs on the SL using hydrothermal method [18–21], and discuss how to realize size tuned NWs with needed morphology.

2. Experiments

Firstly, a direct current (DC) and radio frequency (RF) co-sputtering method was used to deposit ZnO thin film (particle size changing from ~5 to 46 nm) on the cleaned Si (1 0 0) substrate. The samples with the growth time of 5, 10, 15 and 30 min were denoted as $a-$, a, $a+$ and A, respectively (Table 1). After the growth, sample a was cut into four pieces, in which three pieces were annealed at 600, 800 and 1000 °C in air for 30 min and were denoted as b, c and d, respectively. Sample A, which was processed with the same procedure, denoted as B, C and D, respectively (Table 1).

Secondly, ZnO NWs were fabricated on the substrates a, b, c, d, A, B, C and D by hydrothermal method using $Zn(CH_3COO)_2 \cdot 2H_2O$ and $C_6H_{12}N_4$ as reaction source, the reaction solution was adjusted to identical concentration (0.01 mol/L). Then the reaction kettle was put into an oven and maintained at 90 °C for 24 h. The obtained samples were denoted as a', b', c', d', E, F, G and H (Table 1). ZnO NWs, which were grown on substrate a under the same conditions mentioned above except that the solution concentration was adjusted to 0.001 mol/L was denoted as a''. Sample A annealed at 1000 °C in Ar gas for 30 min was explored as SL for growing NWs, the obtained sample was denoted as H' (Table 1).

* Corresponding author. Tel.: +33 238255378; fax: +33 238255376.
E-mail address: caroline.andreazza@univ-orleans.fr (C. Andreazza-Vignolle).

0921-4526/$ - see front matter © 2011 Elsevier B.V. All rights reserved.
doi:10.1016/j.physb.2011.03.031

Table 1
Detailed parameters for the sub-layers and homo-epitaxial nanowires.

Sample name	Time deposition (min)	Layer thickness (nm)	Particle size (nm)	Annealing temperature (°C)/atmosphere	Sample name after NW elaboration	Concentration (mol/L)
a-	5	5	5	–	–	–
a	10	10	10	–	*a*′	0.01
a	10	10	10	–	*a*″	0.001
a+	15	20	20	–	–	–
A	30	70	46	–	*E*	0.01
b	10	10	20	600 °C/air	*b*′	0.01
c	10	10	15	800 °C/air	*c*′	0.01
d	10	10	–	1000 °C/air	*d*′	0.01
B	30	70	68	600 °C/air	*F*	0.01
C	30	70	81	800 °C/air	*G*	0.01
D	30	70	138	1000 °C/air	*H*	0.01
	30	70	140	1000 °C/Ar	*H*′	0.01

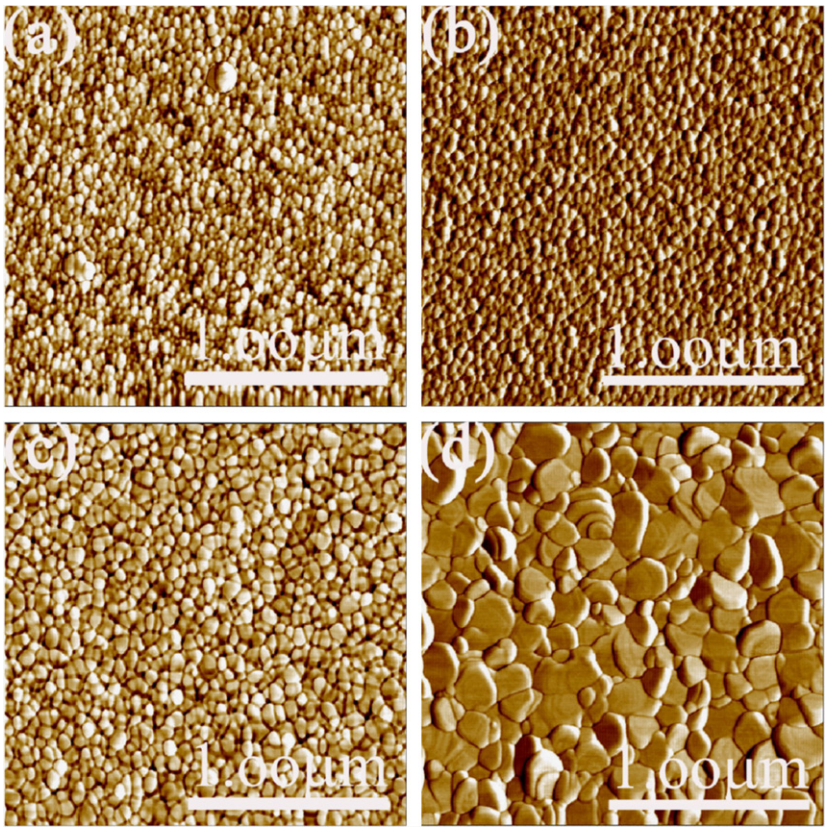

Fig. 1. AFM images of samples *A*, *B*, *C* and *D*: (a) as-grown SL, (b)–(d) SLs annealed at 600, 800 and 1000 °C, respectively.

The surface morphology of the samples was investigated by field emission scanning electron microscopy (FESEM) and atomic force microscopy (AFM); the composition was measured by the energy dispersive X-ray spectrometry (EDX) and Rutherford back-scattering spectrometry (RBS), the crystal structure was examined by X-ray diffraction (XRD) and transmission electron microscopy (TEM) in high resolution mode coupled with selected area electron diffraction (SAED).

3. Results and discussion

3.1. Morphological and structural characteristics of ZnO SLs

The SEM images (not shown here) of the as-grown ZnO samples *a*−, *a* and *a*+ fabricated by magnetron sputtering with the growth time of 5, 10 and 15 min, respectively, show that the SLs are composed of particles. The average particle size increases with deposition time from ∼5, ∼10, ∼20, to 46 nm for samples obtained with deposition time changing from 5, 10, 15 to 30 min, respectively. Fig. 1 shows AFM images of the as-grown sample *A* and the corresponding annealed samples at 600, 800 and 1000 °C under air for 30 min. When the SL was annealed, the particle size became larger with increasing annealing temperature. Clear grain like structure was observed for these images with an average size of 46, 68, 81 and 138 nm for the samples *A*–*D*. For sample *D* larger size dispersion was observed.

To explore structural properties of the as-grown and annealed SLs, XRD experiments were performed as shown in Fig. 2. Only one peak corresponding to the (0 0 2) plane is observed in the X-ray spectra for all the samples indicating that all samples are highly *c*-axis oriented with the (0 0 2) plane parallel to the

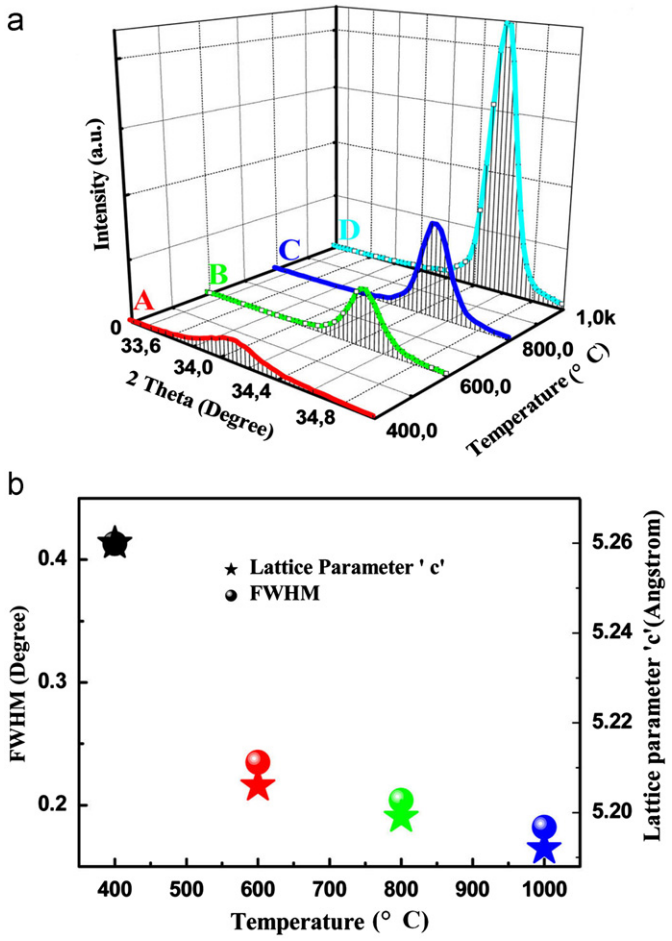

Fig. 2. XRD pattern of (a) *A–D* samples with (b) corresponding 'c' lattice parameter and FWHM values versus temperature.

substrate. This behavior is due to the lowest surface energy of the (0 0 1) basal plane in ZnO. The (0 0 2) peak position of the reference ZnO powder is $2\theta = 34.45^\circ$ [22]. The diffraction peak position of the as-grown ZnO SL (Table 2) is less than the powder value indicating that the film is in a uniform state of strain with expansion components parallel to the *c*-axis. It is also observed that the peak position of (0 0 2) plane shifts close to the powder value when the annealing temperature is at 600 °C. This peak position starts to shift into larger degree compared to the powder value when the annealing temperature is at 800 and 1000 °C. If this macro-strain was only due to residual stress effect induced by the growth method, the initial stress in the as-grown sample would be in one direction and changes into an opposite direction after annealing at higher temperature.

The calculated values of the lattice constant are listed in Table 2. The large value of the lattice parameter "*c*" for the as-grown films compared with the unstressed powder value shows that the unit cell is elongated along the *c*-axis, and compressive force acts in the plane of the film. The compressive force almost disappeared at an annealing temperature of 600 °C resulting in a decrease in "*c*" value. Considering isotropic stress components in the film plane and no out-of-plane stress components (biaxial state), the in-plane stress σ can be expressed from the out-of-plane strain value e_{zz} as Segmüller and Murakami reported [23]:

$$\sigma = [c_{13} - (c_{11} + c_{12})c_{33}/2^* c_{13}]e_{ZZ}, \quad (1)$$

$$e_{ZZ} = (c - c_0)/c_0, \quad (2)$$

where c_{ij} are the elastic stiffness constants of ZnO [24], c is the lattice parameter obtained from the (0 0 2) peak position and c_0 corresponds to the free stressed and stoichiometric value. According to Eqs. (1) and (2), the residual stress of our as-grown and annealed buffer layers could be calculated and summarized in Table 2. Stress in ZnO films contains a thermal component and an intrinsic component. The thermal stress is the result of the difference between the thermal expansion coefficient of the coating and the substrate [25]. The thermal expansion coefficient of ZnO is larger than that of silicon, resulting in a tensile lateral stress in the ZnO film due to cooling after deposition. Considering the substrate and film expansion coefficients (bulk ZnO: 4.75×10^{-6}/K and bulk Si: 2.59×10^{-6}/K [26]) and the difference between the coating temperature (400 °C) and room temperature, the tensile thermal stress is evaluated around 0.5 GPa. The resulting intrinsic compressive stress (around 2.85 GPa) is a typical behavior in sputtered ZnO thin films and is commonly associated with grain boundaries and interstitial atoms in ZnO lattice due to the 'atomic peening' mechanism originated from energetic species interaction with the growing surface [25]. The difficulty is to separate the strain variation due to the stress relaxation from the oxygen stoichiometry variation. The RBS measurements (Table 2) supported by EDX analysis show that the oxygen atomic concentration is almost constant between the as-grown sample and samples *B* and *C*. These results confirm that the decrease in the *c*-axis parameter is due to annealing, which is a pure mechanical stress relaxation (defects, grains boundaries etc.) as reported by Gupta and Mansingh. [27]. On the contrary, annealing at 1000 °C is a combination of several mechanisms of atom diffusion which induces large re-crystallization process (grain growth and equi-atomic composition state). In this case, the variation of the lattice parameter "*c*" is due to complete stress relaxation and structural rearrangement of the crystalline domain. The variation $\Delta c/c$ for sample *D* with respect to a perfect unstressed sample is of -0.27% which is a very small variation. The domain size has been evaluated from the integral width β of the (0 0 2) and (0 0 4) lines according to the Scherrer's relation [28]:

$$D = K\lambda/[\cos\theta(\beta^2 - \beta_0^2)^{1/2}(\pi/180)] \quad (3)$$

With the Cu–Kα radiation wavelength of $\lambda = 0.15418$ nm, the correction form factor $K = 1$, the diffraction angle θ and the integral peak width β_0 caused by instrumental broadening. The grain size increases from 14 to 23 nm with increase in the deposition time and to 56 nm with increase in the annealing temperature. This process has been suggested by Hickernell [29] as re-crystallization occurring during annealing. SEM observations in cross-section reveal a ZnO layer thickness around 70 nm. This value is close to the domain size (which is an evaluation of the crystalline domain size in the *c*-axis dimension, perpendicular to the substrate surface) obtained in sample *D*.

As observed by AFM, the as-grown ZnO SL was composed of smaller particles, and the particle size became larger after increase in the annealing temperature, this observation indicates that merging processes at the interface occurred and became very important as the temperature increased [30]. Finally, the integral intensity of the (0 0 2) peak is a parameter allowing the evaluation of the preferential orientation of the re-crystallized grains with respect to the substrate. This indicates an optimization of the orientation in addition to an improvement of the crystalline quality.

Table 2
XRD structural analysis (non-resolved $K\alpha$ doublet) and RBS/EDX composition measurement results of samples *a*, *A*, *B*, *C* and *D*. RBS measurements give an absolute value of oxygen concentration while EDX is given as a relative value to the as-grown sample (sample A).

Sample	$2\theta_{max}$ ± 0.01 (deg.)	Integral area $\pm 5\%$	FWHM β ± 0.01 (deg.)	Lattice Parameter *c* (Å)	Stress (GPa) ± 0.1 Gpa	Domain size (nm)	O at% RBS	O% EDX
a	33.98	1107	0.671	5.270	2.79	14		
A	34.08	2270	0.413	5.260	2.35	23	48.5	0
B	34.45	2960	0.235	5.206	0	39	49	0
C	34.49	3390	0.204	5.199	0.30	45	49	0
D	34.54	6780	0.182	5.192	0.61	56	50	+3
Unstress	34.45	–	–	5.206	0	–	50	–

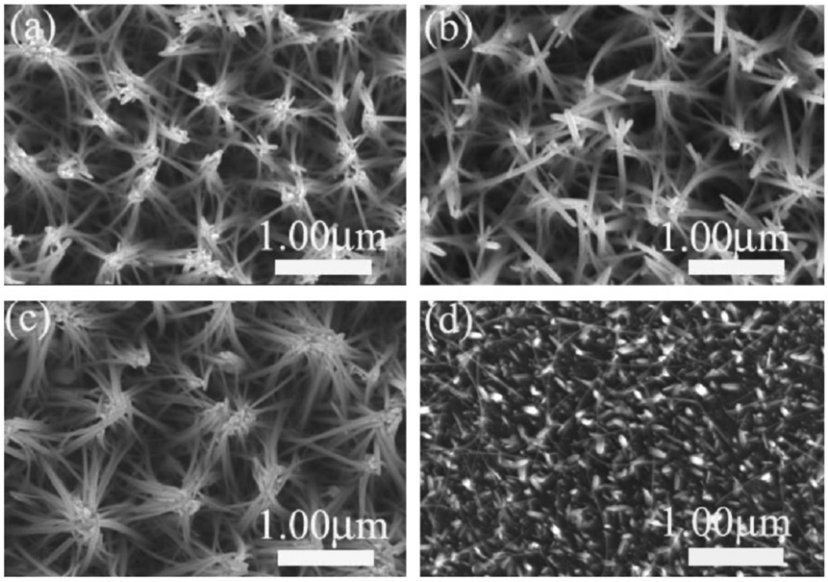

Fig. 3. (a–d) SEM images of samples *a′*, *b′*, *c′* and *a″*.

3.2. Morphological and structural characteristics of Homo-epitaxial ZnO nanostructures on ZnO SLs

Two series of samples have been explored (Table 1): the first ones were grown on 10 nm thick as-grown and annealed SL (the samples are denoted *a′*, *b′*, *c′*, *d′* and *a″* as described above), the second ones were on 70 nm thick as-grown and annealed SLs (the samples are denoted *E*, *F*, *G*, *H* and *H′* as described above).

Fig. 3(a–c) shows top view SEM images of samples *a′*, *b′* and *c′*, top agglomerate ZnO NWs were observed forming wiring harness like structure for samples *a′*, *b′* and *c′* with the diameter of the NWs around 50 nm. The top agglomerate phenomenon became much more serious while annealing temperature for SL was at 800 °C, and the number of NWs forming one wiring harness increases from around 15 to around 30 wires for samples *a′* and *c′*, respectively. Nothing was obtained for sample *d′* (not shown here), which may be due to the phase transition of the thin SL under higher annealing temperature at 1000 °C [O:Zn=71:29 (atom ratio) for the substrate]. To get smaller diameter NWs, the solution concentration has been lowered to 0.001 mol/L for sample *a″*. As shown in Fig. 3(d), besides wires with larger diameter of about 30 nm, ultrafine ZnO NWs with a diameter of ~11 nm with large aspect ratio (~200 for the longest NWs) were obtained.

Concerning the ZnO NWs obtained on thicker SLs (thickness=70 nm), top view and corresponding cross-section SEM images of the ZnO NWs fabricated on the substrates *A*, *B*, *C* and *D* are shown in Fig. 4, which indicate that the thickness of the SL could influence the morphology of the ZnO NWs; the intensity of the (0 0 2) peak enhanced with increasing the thickness of the SL in the XRD pattern (not shown here). When the thickness of the SL reaches 70 nm, the NWs did not agglomerate anymore and became highly oriented. For samples *E–H*, aligned ZnO NWs were obtained. The images of sample *H* showed that the alignment is much better compared with the others. It seems that the annealing process has an important effect on the growth of the NWs: the thicker SL contributed to the better growth orientation, and the larger grain size of the SL resulted in the bigger diameter of the NWs. The average diameter of the NWs was about 60, 73, 77 and 146 nm for the samples *E*, *F*, *G* and *H* respectively. These results illustrate that the morphology of the NWs can be affected by the thickness of the SL, and the diameter of epitaxial NWs can be tuned by the particle size of the SL. The average length is about 2.2, 2.1, 1.8 and 1.3 μm for samples *E*, *F*, *G* and *H*, respectively. It is evident that sample *H* owning much shorter length compared with others may be due to larger diameter leading to lower growth rate along the *c*-axis.

TEM image (Fig. 5) of sample *H* shows a nanoneedle-like structure with large root and small tip. The HR-TEM and SAED (insets) showed that the NWs are single crystalline. The lattice fringes are perpendicular to the wire axis indicating that the ZnO NW grew along the [0 0 1] direction. Moreover, the interplanar distance measured along the NW is equal for both the root and the tip. It means that lattice parameter "*c*" is uniform along

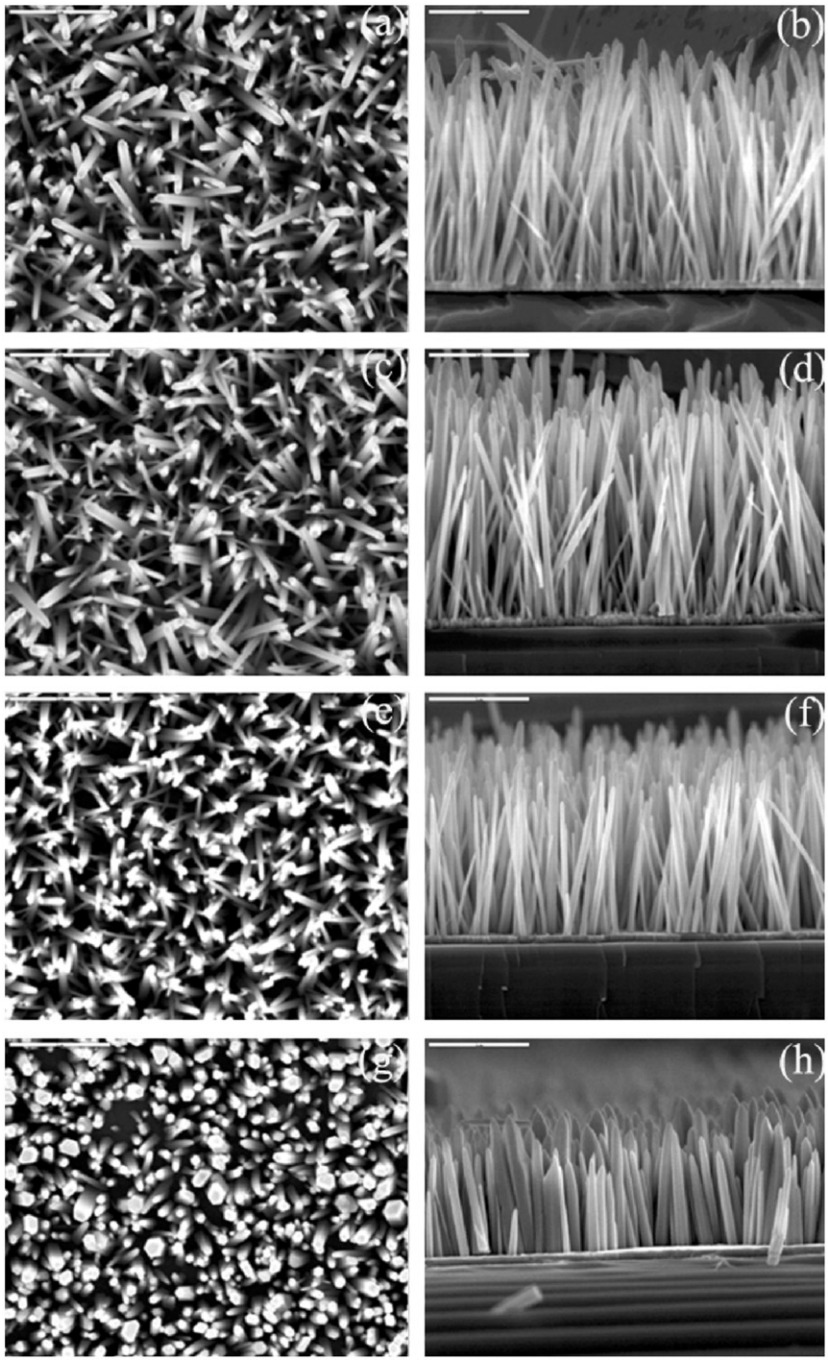

Fig. 4. (a,b), (c,d), (e,f) and (g,h) top view and cross-section SEM images of samples *E*, *F*, *G* and *H*, respectively, The scale bar is 1 μm.

the whole NW. These results demonstrate the homo-epitaxial growth of the *c*-axis oriented ZnO NWs onto the *c*-axis oriented SL.

In order to control the growth rate of the NWs, the SL *A* annealed at 1000 °C in the Ar gas for 30 min was explored; similar results as sample *D* were obtained in terms of the particle size, lattice parameter, stress value and domain size for the annealed SL, the corresponding AFM image of the annealed SL was shown in Fig. 6(a). In order to grow NWs on this kind of SL by hydrothermal method, the solution concentration of 0.01 mol/L for both $Zn(CH_3COO)_2 \cdot 2H_2O$ and $C_6H_{12}N_4$ was used, and the reaction kettle was put into an oven and maintained at 90 °C for 24 h. The top view and cross-section SEM images of the NWs are shown in Fig. 6(b–c), the obvious difference is that the length of the NWs for sample *H′* is more than two times longer compared with that for sample *H*.

4. Conclusion

In summary, the size (diameter and length) of the epitaxial NWs could be tuned under proper conditions by hydrothermal method. The diameter of the NWs is greatly influenced by the particle size of the SL and solution concentration, so we believe that the diameter of the homo-epitaxial NWs in accordance with the same value as the particle size of the SL under optimal

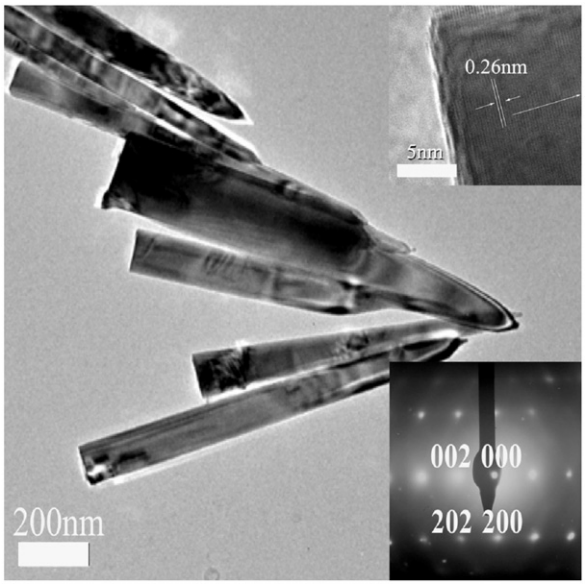

Fig. 5. TEM image of the ZnO NWs (sample *H*) with the HR-TEM image (upper trace) and the SAED (lower trace) of the NW shown in the insets.

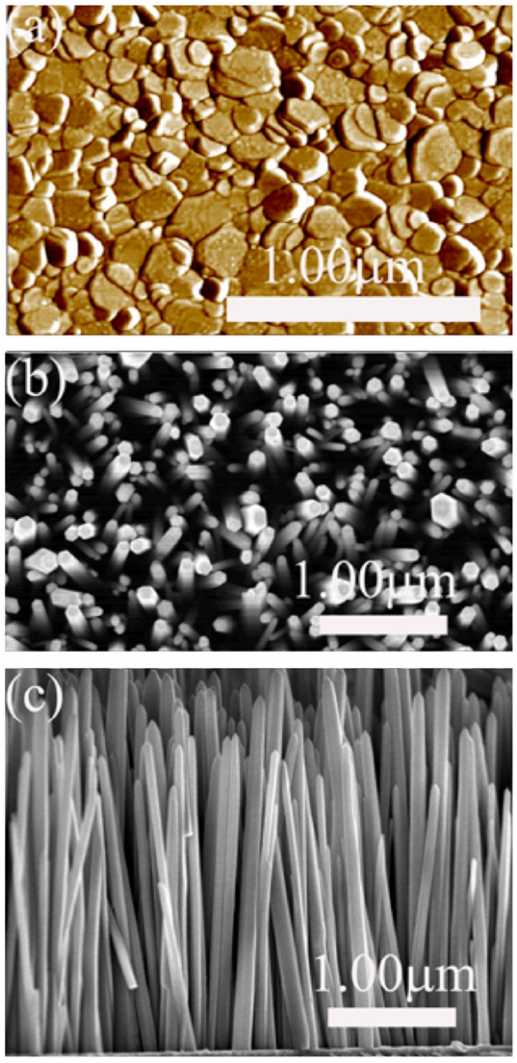

Fig. 6. (a) AFM image ZnO SL annealed at 1000 °C in Ar gas for 30 min, (b) and (c) top morphology and cross-section SEM images of the NWs for sample *H′* fabricated on the corresponding SL, respectively.

conditions could be realized. The polarity surface will strongly influence the growth rate of the epitaxial NWs; thus we could tune the size of the ZnO NWs through adjusting of growth conditions.

Acknowledgment

The authors would like to thank M. Vayer and F. Warmont from CRMD for AFM images. This work was also supported by the Key Project of National Natural Science Foundation of China under Grant no. 50532050, the "973" program under Grant nos. 2006CB604906 and 2008CB317105, the Innovation Project of Chinese Academy of Sciences and the National Natural Science Foundation of China under Grant nos. 60506014, 10674133 and 60776011.

References

[1] W.Y. Liang, A.D. Yoffe., Phys. Rev. Lett. 20 (1968) 59.
[2] C.J. Lee, T.J. Lee, S.C. Lyu, Y. Zhang, H. Ruh, H.J. Lee., Appl. Phys. Lett. 81 (2002) 3648.
[3] L.B.K. Law, J.T.L. Thong., Appl. Phys. Lett. 88 (2006) 133114.
[4] L. Vayssieres, K. Keis, A. Hagfeldt, S.E. Lindquist., Chem. Mater. 13 (2001) 4386.
[5] J.C. Johnson, H.Q. Yan, P. Yang, R.J. Saykally., J. Phys. Chem. B 107 (2003) 8816.
[6] M.H. Huang, S. Mao, H. Feick, H. Yan, Y. Wu, H. Kind, E. Weber, R. Russo, P. Yang, Science 292 (2001) 1897.
[7] H. Kind, H. Yan, B. Messer, M. Law, P. Yang., Adv. Mater. (Weinheim, Ger.) 14 (2002) 158.
[8] H. Yan, J. Johnson, M. Law, R. He, K. Knutsen, J.R. McKinney, J. Pham, R. Saykally, P. Yang., Adv. Mater. (Weinheim, Ger.) 15 (2003) 1907.
[9] W.I. Park, G.-C. Yi, M. Kim, S.J. Pennycook, Adv. Mater. 14 (2002) 1841.
[10] C.J. Lee, T.J. Lee, S.C. Lyu, Y. Zhang, H. Ruh, H.J. Lee, H.W. Shim, E.-K. Suh, C.J. Lee, Chem. Phys. Lett. 363 (2002) 134.
[11] P.X. Gao, Y. Ding, Z.L. Wang, Nano Lett. 3 (2003) 1315.
[12] S.W. Kim, S. Fujita, Appl. Phys. Lett. 86 (2005) 153119.
[13] L.E. Greene, B.D. Yuhas, M. Law, D. Zitoun, P.D. Yang, Inorg. Chem. 45 (2006) 7535.
[14] C.H. Bae, S.M. Park, S.E. Ahn, D.J. Oh, G.T. Kim, J.S. Ha, Appl. Surf. Sci. 253 (2006) 1758.
[15] Z.Y. Fan, D. Dutta, C.J. Chien, H.Y. Chen, E.C. Brown, Appl. Phys. Lett. 89 (2006) 213110.
[16] D. Zhao, C. Andreazza-Vignolle, P. Andreazza, J. Ma, Y. Liu, D. Shen, Chem. Phys. Lett. 399 (2004) 522.
[17] Y. Zhang, R.E. Russo, S.S. Mao, Appl. Phys. Lett. 87 (2005) 133115.
[18] D. Zhao, C. Andreazza-Vignolle, P. Andreazza, J. Ma, Y. Liu, D. Shen, Chem. Phys. Lett. 408 (2005) 335.
[19] W. Wu, G. Hu, S. Cui, Y. Zhou, H. Wu, Cryst. Growth Design 11 (2008) 4014.
[20] J.S. Huang, C.F Lin, J. Appl. Phys 103 (2008) 014304.
[21] J. Qiu, X. Li, W. He, S-J Park, H.K. Kim, Y.H. Hwang, J.H. Lee, Y.D. Kim, Nanotechnology 20 (2009) 155603.
[22] American Standard for Testing of Materials (ASTM), 36,1451.
[23] A. Segmüller, M. Murakami, in: K.N. Tu, R. Rosenberg (Eds.), Analytical Techniques for Thin Films, Acad, Boston, 1988, p. 143.
[24] T.B. Bateman, J. Appl. Phys. 33 (1962) 3309.
[25] H.W. Lee, S.P. Lau, Y.G. Wang, B.K. Tay, H.H. Hng, Thin Solid Films. 458 (2004) 1 15.
[26] S.M. Sze, Semiconductor Devices Physics and Technology, Wiley, 2002, p. 538.
[27] Vinay Gupta, Abhai Mansingh, J. Appl. Phys. 80 (1996) 1063.
[28] H.P. Klug, L.E. Alexander, X-Ray Diffraction Procedures for Polycrystalline and Amorphous Materials, Wiley, New York, 1974, p. 687.
[29] F. S. Hickernell, MRS Spring Meeting San Francisco, California, 1985.
[30] E. Cetinörgü, S. Goldsmith, R.L. Boxman, Surf. Coat. Tech. 201 (2007) 7266.